mater.scichina.com link.springer.com Published online 12 April 2024 | https://doi.org/10.1007/s40843-023-2783-1

Cu_2O as the hole extraction layer modified $BiVO_4$ photoanode to enhance charge separation and transfer

Ze Tian[1], Zhenxia Wang[1], Zizai Ma[2,3*], Jinping Li[3] and Xiaoguang Wang[1,3*]

ABSTRACT **Photoinduced charge separation and transfer are the core factors affecting the photoelectrochemical performance of $BiVO_4$-based photoanodes. Herein, a hole extraction layer was inserted between a $BiVO_4$ photoanode and an oxygen evolution cocatalyst (OEC). The introduction of Cu_2O as a hole extraction layer between the OEC layer (FeOOH/NiOOH) and $BiVO_4$ optimized the migration paths and extended the lifetimes of the photogenerated holes, thus enhancing the photoelectrochemical performance of the photoelectrode. The charge separation efficiency of the optimized $BiVO_4/Cu_2O$/FeOOH/NiOOH photoanode was 92.0% significantly higher than the 70.6% efficiency for pure $BiVO_4$. As expected, this photoanode also displayed a high photocurrent density of 3.85 mA cm^{-2} at 1.23 V_{RHE} (under AM 1.5G illumination), which was 2.77 times greater than that of pure $BiVO_4$. Our results indicate that electrodepositing a Cu_2O hole extraction layer is a simple and scalable method for increasing the photoelectrochemical activity of $BiVO_4$ photoanodes for solar water splitting.**

Keywords: $BiVO_4$, Cu_2O, hole extraction layer, solar water splitting

INTRODUCTION

The energy crisis and environmental degradation are becoming increasingly serious worldwide. Hydrogen energy is clean and renewable energy, and it has received widespread attention [1,2]. In 1972, Fujishima and Honda [3] discovered that TiO_2 electrodes could produce hydrogen *via* water splitting under irradiation. Since then, photoelectrochemical (PEC) water splitting has attracted increasing interest as a promising and environmentally friendly method for solar hydrogen production [4,5]. In the PEC reaction, the photoelectrode absorbs light to generate holes and electrons, which are then separated and transferred, followed by water oxidation and reduction reactions. The water splitting reaction is an extremely energy-intensive uphill reaction [6]. In addition, the anodic water oxidation process occurs at the contact interface between the anode and the electrolyte solution *via* a four-electron transfer process ($2H_2O + 4h^+ \rightarrow O_2\uparrow + 4H^+$), which is the main limiting step of the water oxidation reaction [7]. Therefore, the development of photoanodes with high efficiencies and low costs is crucial for constructing high-performance and commercially viable PEC devices.

Through the continuous efforts of researchers in recent years, several highly efficient semiconductors, such as WO_3 [8,9], TiO_2 [10,11], Fe_2O_3 [12,13], Ta_3N_5 [14,15] and $BiVO_4$ [16–18] have emerged as photoanodes. To date, monoclinic scheelite $BiVO_4$ is the ideal candidate for photoanodes [19,20], which has the advantages of a small band gap (~2.4 eV), suitable edge position, low initial potential and abundant synthetic elements [21–24]. Under AM 1.5G illumination, the maximum theoretical photocurrent density of $BiVO_4$ photoanode reached 7.5 mA cm^{-2} [25], and the theoretical conversion efficiency for solar energy hydrogen production (STH) reached 9.1% [26]. However, due to poor electrical conductivities, short carrier diffusion lengths and slow water oxidation kinetics, $BiVO_4$ photoanodes suffer from severe charge recombination both in the bulk and at the interface during PEC water splitting, which is the main problem limiting the use of $BiVO_4$ [27]. The deposition of oxygen evolution cocatalysts (OECs) such as CoPi [28], NiOOH [29], FeOOH [30], CoOOH [31] and $NiFeO_x$ [32] accelerated the kinetics of aqueous oxidation (surface charge transfer) on the surface of $BiVO_4$. According to the literature, modification of the cocatalysts overcomes the sluggish water oxidation kinetics and thus inhibits the recombination of the photogenerated charges at the photoanode/electrolyte interface. However, this strategy generates new recombination centres at the semiconductor/cocatalyst interface, which in turn deteriorates the water oxidation capacities of the PECs [33,34].

In this case, it is imperative to modulate the interface of the photoanode by introducing a hole extraction layer. It serves as a hole reservoir and/or hole mediator at the interface, thus reducing undesirable interfacial charge recombination. For example, Domen and coworkers [35] constructed a p-n junction by loading p-NiO on the OEC/$BiVO_4$ surface, which facilitated rapid transfer of the holes and increased the rate of water oxidation. In addition, other p-type semiconductors, such as Co_3O_4 [36], MoS_2 [37], and $BiFeO_3$ [38], also provided hole extraction and water oxidation in various photoanodes. As a narrow-band-gap (2.0 eV) p-type semiconductor, the valence band (VB) of Cu_2O is located between the conduction band (CB) and the VB of bare $BiVO_4$, and its CB is more negative than that of $BiVO_4$ [39]. Therefore, the development of Cu_2O as a hole extraction layer for $BiVO_4$ photoanodes is desirable.

Herein, we proposed a feasible method for synthezing a $BiVO_4$

[1] Laboratory of Advanced Materials and Energy Electrochemistry, Institute of New Carbon Materials, College of Material Science and Engineering, Taiyuan University of Technology, Taiyuan 030024, China
[2] College of Chemistry, Taiyuan University of Technology, Taiyuan 030024, China
[3] Shanxi Key Laboratory of Gas Energy Efficient and Clean Utilization, Taiyuan University of Technology, Taiyuan 030024, China
* Corresponding authors (emails: mazizai@tyut.edu.cn (Ma Z); wangxiaoguang@tyut.edu.cn (Wang X))

photoanode with a Cu_2O hole extraction layer for PEC water oxidation. A Cu_2O layer was introduced by facile electrodeposition, which was expected to ensure rapid separation and transport of the photogenerated carriers. Finally, after loading the water oxidation cocatalyst, the $BiVO_4/Cu_2O/FeOOH/NiOOH$ photoanode exhibited a photocurrent density of 3.85 mA cm^{-2} at 1.23 V_{RHE}, which was 2.77 times greater than that of pure $BiVO_4$.

EXPERIMENTAL SECTION

Chemicals and reagents

Bismuth nitrate pentahydrate ($Bi(NO_3)_3{\cdot}5H_2O$, ⩾99.0%), potassium iodide (KI, ⩾99.0%), *p*-benzoquinone ($C_6H_4O_2$, 97.0%), vanadyl(IV)-acetylacetonate ($C_{10}H_{14}O_5V$, 98.0%), methyl sulfoxide (C_2H_6OS, >99.0%), copper(II) sulfate ($CuSO_4$, 99.0%), iron (II) sulfate hydrate ($FeSO_4{\cdot}7H_2O$, ⩾99.0%), ethyl alcohol (C_2H_6O, 99.5%), and sodium hydroxide (NaOH, 97.0%) were obtained from Shanghai Aladdin Biochemical Technology Co., Ltd.

Preparation of photoanodes

$BiVO_4$ photoanodes were prepared by electrodeposition and annealing methods [40]. $BiVO_4/Cu_2O$ photoanodes were obtained by electrodeposition of Cu_2O with varying composite quantities on the surface of $BiVO_4$. The 0.4 M $CuSO_4$, 3 M lactic acid and 4 M NaOH were dissolved in deionized water as electrolytes. The solution is kept at 35°C to generate single-phase Cu_2O [41]. The three-electrode system was adopted, with the prepared $BiVO_4$ as the working electrode, the Pt sheet as the counter electrode, and Ag/AgCl as the reference electrode, and the potential was deposited at −0.5 $V_{Ag/AgCl}$, with charges of 0.015, 0.02, and 0.025 C cm^{-2}, respectively. The FeOOH/NiOOH OEC layer was prepared using photo-assisted electrodeposition, which was deposited separately for 6 min [42].

Characterization

The crystal structure of the photoanodes was characterized by an X-ray diffractometer (XRD, DX-2700) at 40 kV and 30 mA with a Cu Kα radiation source (λ = 0.15406 nm). Scanning electron microscopy (SEM, FEI QUANTA FEG250), transmission electron microscopy (TEM, FEI Tecnai G2 F30), and energy dispersion X-ray analyzer (EDX) were used to characterize the morphology of the photoanodes and the elemental distribution of the photoanodes. The optical property measurements were conducted on an ultraviolet-visible (UV-vis) spectra photometer (UV-9000S). The surface composition and elemental chemical state of the photoanodes were detected by X-ray photoelectron spectroscopy (XPS, Thermo Scientific ESCALAB 250Xi) with Al Kα radiation at 12.5 kV and 16 mA. All binding energies were calibrated according to reference energy of C 1s (284.8 eV).

PEC performance measurement

The measurement and analysis of PEC performance was performed on the VSP-3e electrochemical workstation. The prepared photoanodes were used as the working electrode, a Pt plate and an Ag/AgCl electrode were used as the counter and the reference electrodes, respectively. Illumination was offered by a xenon lamp (MC-X301B) equipped with AM 1.5G filter, the intensity was calibrated to 100 mW cm^{-2} by standard reference of a Newport 91150 silicon solar cell, and the irradiation area of all measurements was 1 cm^2. Most experiments were performed in 0.5 M potassium borate buffer solution, and some with 1 M Na_2SO_3 was added into the electrolyte to compare photocurrents obtained from sulfite and water oxidation. All potentials are given *versus* reversible hydrogen electrode (RHE) using the RHE calibration: $E_{RHE} = E_{Ag/AgCl} + 0.059pH + 0.197$, where pH is 9.3 in the electrolyte measured by the pH meter (Fig. S1). The scanning rate measured by linear scanning voltammetry was 10 mV s^{-1}. The incident photon-to-electron conversion efficiency (IPCE) was also tested at 1.23 V_{RHE} under the three-electrode system described above. Electrochemical impedance spectroscopy (EIS) was performed at 0.8 V_{RHE} in the frequency range of 10^{-1}–10^5 Hz with an amplitude of 10 mV. The Mott–Schottky plots were measured in the dark state at the frequency of 1 kHz.

RESULTS AND DISCUSSION

Structure and morphology of photoanodes

The XRD patterns of $BiVO_4$, Cu_2O, $BiVO_4/Cu_2O$, and $BiVO_4/Cu_2O/FeOOH/NiOOH$ were shown in Fig. 1. The main diffraction peaks of pure $BiVO_4$ were 18.9°, 28.9°, 30.5°, 40.0°, and 47.3°, corresponding to (001), (112), (004), (−121), and (024) crystal planes, respectively. It indicated that the prepared $BiVO_4$ was the monoclinic phase with scheelite structure (PDF#97-003-3243), which had a unique Bi 6s electronic structure with O 2p hybridization and the asymmetry of BiO_8 polyhedral [43]. The peaks at 36.8° and 42.8° were indexed to the (111) and (200) crystal planes of the Cu_2O (PDF#97-062-8619) [41]. Likewise, the corresponding peak of $BiVO_4/Cu_2O$ indicated that Cu_2O was successfully deposited on the surface of $BiVO_4$ photoanode. In addition, the XRD pattern of $BiVO_4/Cu_2O/FeOOH/NiOOH$ was quite similar to the prepared $BiVO_4/Cu_2O$, and no diffraction peaks corresponding to FeOOH and NiOOH were observed, which may be due to the fact that FeOOH and NiOOH are thin and amorphous.

Fig. 2a, b show the SEM images of $BiVO_4$, which exhibited a wormlike structure uniformly grown on the fluorine-doped tin oxide substrate (FTO). Furthermore, Cu_2O nanoparticles anchored on the $BiVO_4$ *via* electrodeposition were clearly observed as shown in Fig. 2c, d, and the sizes of the Cu_2O

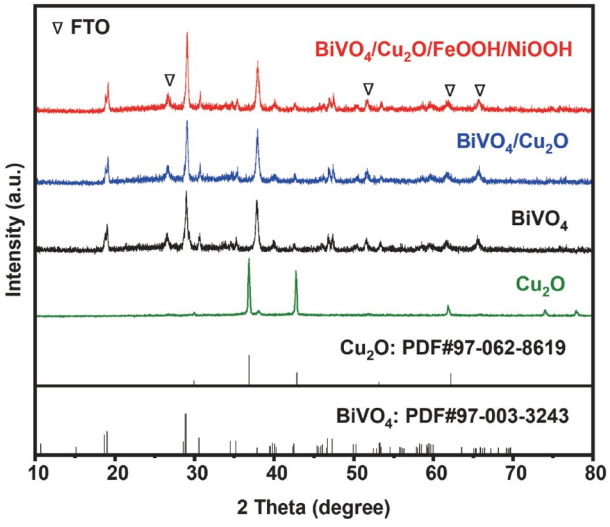

Figure 1 XRD patterns of Cu_2O, $BiVO_4$, $BiVO_4/Cu_2O$, and $BiVO_4/Cu_2O/FeOOH/NiOOH$ photoanodes.

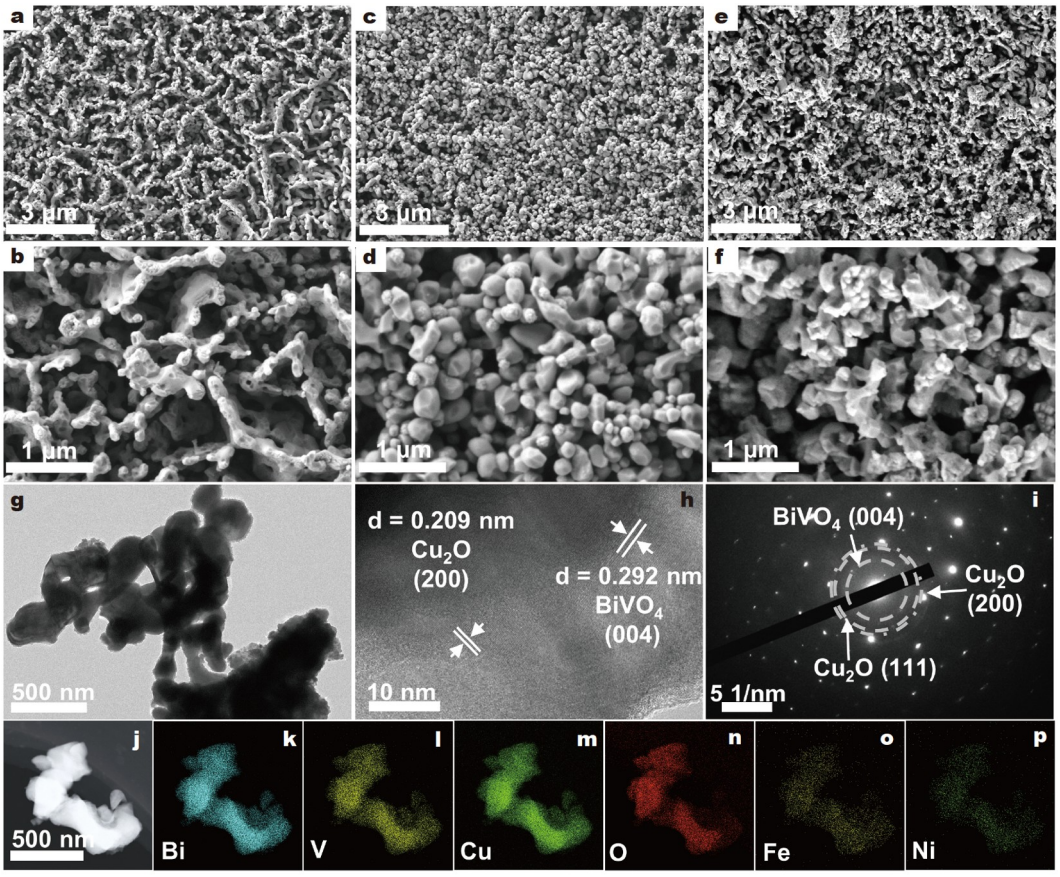

Figure 2 SEM images of (a, b) pure $BiVO_4$, (c, d) $BiVO_4/Cu_2O$, and (e, f) $BiVO_4/Cu_2O$/FeOOH/NiOOH photoanodes; (g) TEM, (h) HRTEM, and (i) SAED images of $BiVO_4/Cu_2O$/FeOOH/NiOOH photoanode; (j) STEM image and (k–p) elemental mappings of Bi, V, Cu, O, Fe, and Ni, respectively.

particles ranged from 100 to 200 nm [44]. Fig. 2e, f display the electrode after deposition of the FeOOH/NiOOH OEC layer, and there were obvious particles on the surface of the electrode, with almost no significant change in the sizes of the particles. However, these particles became relatively rough, which proved that the FeOOH/NiOOH OEC layer was deposited on the surface of $BiVO_4/Cu_2O$ [45].

In addition, more detailed microstructural information was obtained with TEM. As shown in Fig. 2g, a typical wormlike morphology was identified, and it was clear that the nanoparticles were attached to the $BiVO_4$, which was consistent with the SEM. The high-resolution TEM (HRTEM) image (Fig. 2h) clearly depicted lattice fringes with different orientations. The spacings of 0.209 and 0.292 nm corresponded to the (200) lattice plane of Cu_2O in the cubic structure and the (004) lattice plane of $BiVO_4$ in the monoclinic phase, respectively. The selected area electron diffraction (SAED) images also indicated the presence of $BiVO_4$ and Cu_2O. The close contact between $BiVO_4$ and Cu_2O was very important in accelerating charge separation and transmission [46]. As shown in Fig. S2, the deposited FeOOH/NiOOH OEC layer was amorphous and had thicknesses of approximately 20–30 nm. The elemental mappings (Fig. 2j–p) demonstrated the presence of Bi, V, Cu, O, Fe, and Ni in the $BiVO_4/Cu_2O$/FeOOH/NiOOH photoanode, and their spatial distributions were uniform.

XPS was used to determine the chemical states of the elements contained in the photoanodes. The XPS survey spectrum (Fig. 3a) showed the presence of Bi, V, O, Cu, Fe and Ni in the prepared $BiVO_4/Cu_2O$/FeOOH/NiOOH photoanode. The high-resolution Bi 4f XPS data (Fig. 3b) displayed two peaks centred at 159.0 and 164.3 eV, which corresponded to the Bi $4f_{7/2}$ and Bi $4f_{5/2}$ binding energies, respectively, indicating that Bi was present in the Bi^{3+} oxidation state [47]. Fig. 3c shows the V 2p high-resolution spectrum. Two peaks were located at 516.7 eV (V $2p_{3/2}$) and 524.0 eV (V $2p_{1/2}$), which indicated the V^{5+} oxidation state [48]. In the O 1s XPS spectrum displayed in Fig. 3d, three peaks at 530.0, 531.6 and 532.8 eV were attributed to lattice oxygen (O_L), oxygen vacancies or defects (Ov) and chemically adsorbed or dissociated oxygen (Oc), respectively [49]. Fig. 3e shows that Cu exhibited two peaks at 932.5 and 952.2 eV, indicating the presence of the Cu^{1+} oxidation state [50]. The peaks located at 710.8 and 723.9 eV in the Fe 2p XPS spectrum (Fig. 3f) were assigned to Fe^{2+}, and the other peaks located at 713.1 and 726.2 eV were assigned to Fe^{3+} [51]. In the Ni 2p XPS spectrum in Fig. 3g, the peaks at 855.6 and 873.0 eV were assigned to Ni^{2+}, and the peaks at 856.4 and 873.8 eV were those of Ni^{3+} [52]. Therefore, Cu_2O, FeOOH and NiOOH were deposited on the surface of the $BiVO_4$ photoanode. Notably, the high-resolution XPS spectra of $BiVO_4$ and $BiVO_4/Cu_2O$ exhibited shifts to lower Bi 4f, V 2p and O 1s binding energies (Fig. S3a–c) relative to those for $BiVO_4/Cu_2O$/FeOOH/NiOOH. In contrast, the Cu 2p (Fig. S3d) peaks moved to higher binding energies. These changes indicated interactions between the semiconductors [53].

To reveal the absorption characteristics of the prepared photoanodes, Fig. 4a shows the UV-vis absorption spectra of pure

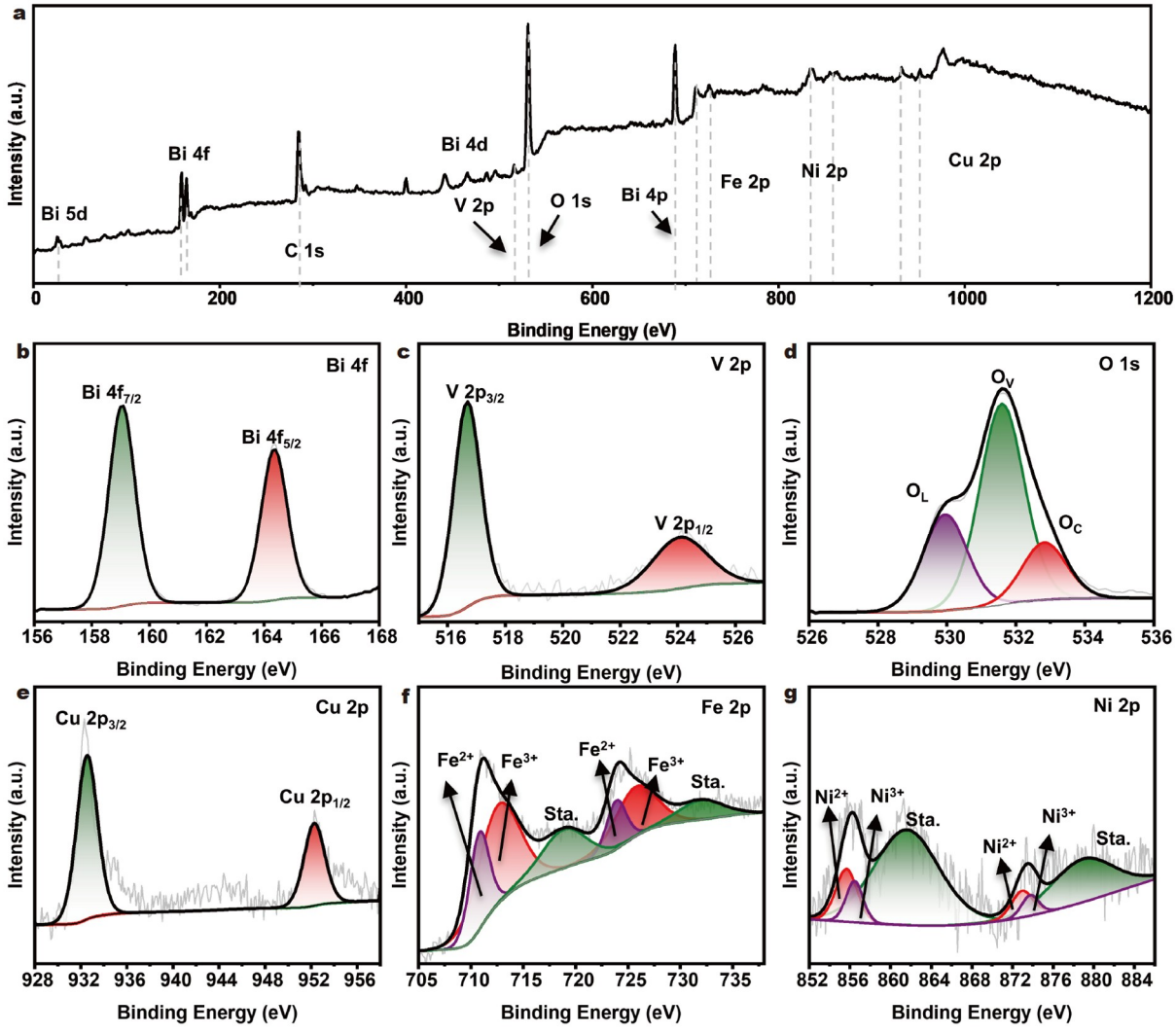

Figure 3 XPS spectra of $BiVO_4/Cu_2O/FeOOH/NiOOH$: (a) survey, (b) Bi 4f, (c) V 2p, (d) O 1s, (e) Cu 2p, (f) Fe 2p, and (g) Ni 2p region.

$BiVO_4$, $BiVO_4/Cu_2O$ and $BiVO_4/Cu_2O/FeOOH/NiOOH$. The peak for $BiVO_4$ in the visible spectrum corresponded to its intrinsic bandgap energy [54]. The band gaps (E_g) of the photoanode were derived with the Tauc equation:

$$\alpha h\nu = A(h\nu - E_g)^{n/2}, \quad (1)$$

where α is the absorption coefficient, $h\nu$ is the photon energy, and A is a constant related to the material properties. Monoclinic $BiVO_4$ and cubic Cu_2O are direct semiconductors and thus the n value is 1 [55].

Fig. 4b shows a bandgap of approximately 2.56 eV for bare $BiVO_4$, which was consistent with that of monoclinic $BiVO_4$ [56]. The bandgaps of the $BiVO_4/Cu_2O$ and $BiVO_4/Cu_2O/FeOOH/NiOOH$ photoanodes remained almost unchanged (approximately 2.55 eV), indicating that Cu_2O, FeOOH and NiOOH made almost no contribution to light adsorption.

Photoanode photoelectric chemical properties

The activities of the photoanodes fabricated for PEC water oxidation were examined by generating the current-potential curves in 0.5 M KBi. The loading of Cu_2O on the $BiVO_4$ nanoarray was preliminarily optimized, as shown in Fig. S4. Fig. 5a shows typical linear sweep voltammetry (LSV) plots for the $BiVO_4$, $BiVO_4/Cu_2O$, and $BiVO_4/Cu_2O/FeOOH/NiOOH$ photoanodes (Cu_2O deposition charge was 0.02 C cm^{-2}). The photocurrent density of the $BiVO_4/Cu_2O/FeOOH/NiOOH$ photoanode reached 3.85 mA cm^{-2} at 1.23 V_{RHE}, which was 2.77 times greater than that for pure $BiVO_4$ (1.39 mA cm^{-2}) and 1.67 times greater than that for $BiVO_4/Cu_2O$ (2.30 mA cm^{-2}). Moreover, compared with those reported previously, the photocurrent density of the $BiVO_4/Cu_2O/FeOOH/NiOOH$ photoanode was relatively high, as shown in Table S1. In addition, the onset potentials of the $BiVO_4/Cu_2O/FeOOH/NiOOH$ and $BiVO_4/Cu_2O$ photoelectrodes were 270 and 411 mV, respectively, which showed considerable negative shifts compared with the 529 mV potential for the $BiVO_4$ photoelectrode. The negative shift in the onset potential was attributed to loading of the surface OEC, which substantially increased the water oxidation capacity of the photoelectrode. More importantly, after depositing the Cu_2O hole extraction layer, it served as a bridge to the surface OEC, increased the charge transfer and separation efficiencies, and thus reduced the overpotential of the PEC reaction.

Furthermore, the IPCEs of the $BiVO_4$, $BiVO_4/Cu_2O$ and $BiVO_4/Cu_2O/FeOOH/NiOOH$ photoanodes were calculated

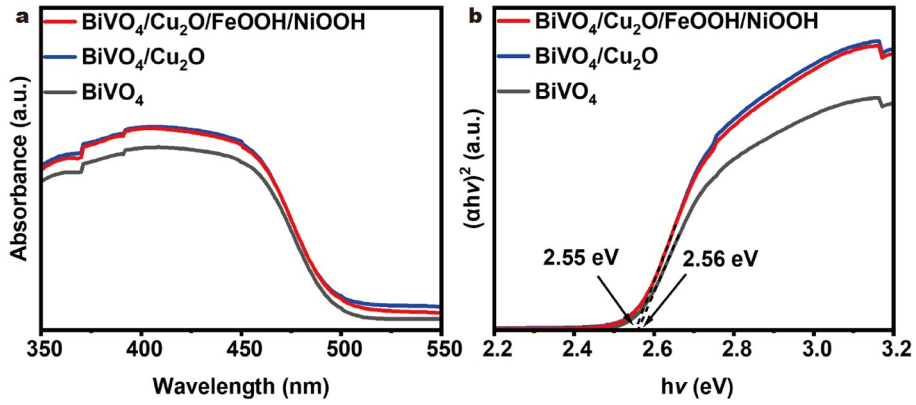

Figure 4 (a) UV-vis absorption spectra and (b) band gap energy of $BiVO_4$, $BiVO_4/Cu_2O$ and $BiVO_4/Cu_2O$/FeOOH/NiOOH photoanodes.

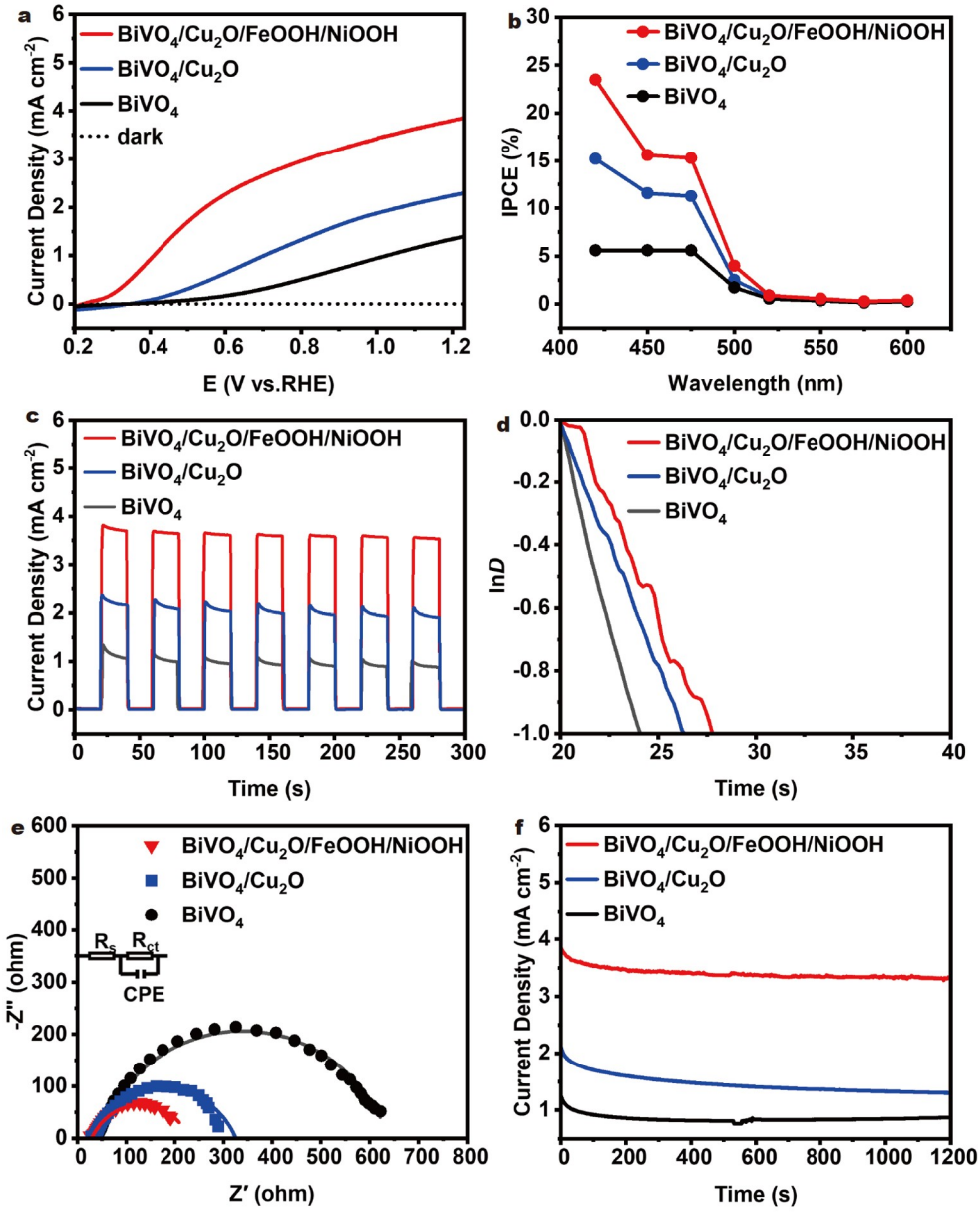

Figure 5 (a) Linear sweep curves, (b) IPCE spectra collected at 1.23 V_{RHE} in 0.5 M KBi, (c) transient photocurrent responses, (d) transient decay time, (e) Nyquist plot at 0.8 V_{RHE} in 0.5 M KBi, and fitted plots (inset is the equivalent circuit used for fitting), and (f) photocurrent stability curves measured in 0.5 M KBi at 1.23 V_{RHE}.

with the following equation:

$$\mathrm{IPCE} = 1240 \times J_{\mathrm{ph}} / \left(\lambda \times P_{\mathrm{light}}\right), \quad (2)$$

where J_{ph} is the optical current density measured at a specific incident wavelength, λ is the wavelength of the incident light, and P_{light} is the power density measured at a specific wavelength [57]. IPCE considers three main processes in PEC cells: light absorption, separation of carriers in semiconductors, and carrier transfer at the semiconductor/electrolyte interface.

As shown in Fig. 5b, after decoration with Cu_2O, FeOOH and NiOOH, the IPCE of the $BiVO_4$ photoanode increased significantly in the absorption wavelength range. The IPCE of the $BiVO_4/Cu_2O$/FeOOH/NiOOH photoanode reached ~23.5%, which was nearly ~1.5 and ~4.2 times greater than those of $BiVO_4/Cu_2O$ (15.2% at 420 nm) and $BiVO_4$ (5.6% at 420 nm), respectively. To investigate the photo responses of the photoanodes over time, typical curves of the chopped transient photocurrent density over time were measured at 1.23 V_{RHE}. During irradiation, the photocurrent increased sharply for all the samples, and once the light was removed, the photocurrent quickly quenched to zero (Fig. 5c). As expected, the photocurrent of the $BiVO_4/Cu_2O$/FeOOH/NiOOH photoanode was significantly increased. In addition, fitting of the carrier decay time to the logarithmic plot of the photocurrent transient response parameter D (ln$D$) revealed the electron-hole pair recombination rate [58]. These results showed that the carrier recombination rate of $BiVO_4/Cu_2O$/FeOOH/NiOOH was relatively low (Fig. 5d), and the transient time of $BiVO_4/Cu_2O$/FeOOH/NiOOH (7.8 s) was 1.2 times longer than that of $BiVO_4/Cu_2O$ (6.4 s) and 1.95 times longer than that of pure $BiVO_4$ (4 s). The synergistic effect of the Cu_2O hole extraction layer and the FeOOH/NiOOH OEC layer slowed charge recombination. The EIS of the three photoanodes tested at 0.8 V_{RHE} in 0.5 M KBi electrolyte are shown in Fig. 5e. The arc radius is related to the charge transfer resistance at the electrode/electrolyte interface; the smaller the radius is, the lower the charge transfer resistance [48]. The parameters extracted from the EIS Nyquist plots are summarized in Table S2. The results showed that the R_{ct} of the $BiVO_4/Cu_2O$/FeOOH/NiOOH photoanode was 200 Ω, which was much smaller than those of $BiVO_4/Cu_2O$ (294 Ω) and $BiVO_4$ (602 Ω). This confirmed that the $BiVO_4/Cu_2O$/FeOOH/NiOOH photoanode provided fast interfacial charge transfer and photoinduced electron-hole pair separation, which were responsible for the significant enhancement in the PEC activity.

The stability of the photoelectrode in water splitting is very important for practical application. An attenuation of the photocurrent densites for the $BiVO_4/Cu_2O$/FeOOH/NiOOH, $BiVO_4/Cu_2O$, and bare $BiVO_4$ photoanodes was measured over time at 1.23 V_{RHE} during AM 1.5G illumination (Fig. 5f). For the bare $BiVO_4$, the photocurrent density decreased from 1.35 to 0.8 mA cm^{-2}, and the steady-state photocurrent was only 59% of the initial value. After 900 s, the photocurrent density-time curve of the $BiVO_4$ photoanode rebounded slightly, indicating that the photoanode may have been corroded during the long reaction. For the $BiVO_4/Cu_2O$ photoanode, the photocurrent decayed by approximately 37.6%, whereas the photocurrent density of the $BiVO_4/Cu_2O$/FeOOH/NiOOH photoanode basically remained at 3.3 mA cm^{-2} after 900 s, and the decay rate was only 13.7%. These results showed that pure $BiVO_4$ was easily corroded by electrolyte, while deposition of the Cu_2O hole-extracted layer promoted charge separation but may have led to the accumulation of holes on the surface, which negatively affected the electrode. With the addition of the FeOOH/NiOOH OEC layer, the hydro-oxygen dynamics were improved, and the holes extracted from Cu_2O were transferred rapidly, thus improving the stability of the photoanode.

To reveal the mechanism for the enhanced PEC performance, we investigated the photoelectric properties and charge transfer kinetics of the $BiVO_4$, $BiVO_4/Cu_2O$, and $BiVO_4/Cu_2O$/FeOOH/NiOOH photoanodes. The light harvesting efficiency (LHE) curves were determined with the following equation:

$$\mathrm{LHE} = 1 - 10^{-A(\lambda)}, \quad (3)$$

where $A(\lambda)$ is the measured absorbance form the UV-vis absorbance spectra and λ is the wavelength of incident light [8].

The trends for the three electrodes in the wavelength range of 350–550 nm were consistent with the UV-vis absorption spectra (Fig. S5a). The photocurrent densities were measured in the presence of a hole scavenger to rule out surface charge recombination (Fig. S5b). The photocurrent densities of the $BiVO_4$, $BiVO_4/Cu_2O$, and $BiVO_4/Cu_2O$/FeOOH/NiOOH photoanodes at 1.23 V_{RHE} were 3.95, 5.2, and 5.4 mA cm^{-2}, respectively.

To evaluate their interfacial processes, the charge separation efficiency (η_{sep}) and transfer efficiency (η_{trans}) of the $BiVO_4/Cu_2O$/FeOOH/NiOOH, $BiVO_4/Cu_2O$, and $BiVO_4$ photoanodes were obtained from J_{max} (Fig. S6) and the following equations:

$$\eta_{\mathrm{sep}} = J_{\mathrm{sul}} / (J_{\mathrm{max}} \times \mathrm{LHE}), \quad (4)$$

$$\eta_{\mathrm{trans}} = J_{\mathrm{H_2O}} / J_{\mathrm{sul}}, \quad (5)$$

where J_{sul} is the photocurrent density in an electrolyte containing a hole scavenger (Na_2SO_3), J_{max} is the maximum photocurrent density, LHE is the light capture efficiency, and J_{H_2O} is the photocurrent density in an electrolyte without a hole scavenger [59].

As shown in Fig. 6a, the addition of a Cu_2O layer significantly increased the η_{sep} of $BiVO_4$ from 70.6% to 88.3%, which was close to that of $BiVO_4/Cu_2O$/FeOOH/NiOOH (92.0%). This indicated that the holes in the $BiVO_4$ nanoparticles were extracted into the Cu_2O layer, resulting in improved charge separation. $BiVO_4/Cu_2O$/FeOOH/NiOOH (Fig. 6b) had a higher charge transport capacity (at 0.87 V_{RHE}, 90.6%) at a relatively low potential than $BiVO_4/Cu_2O$ (at 0.97 V_{RHE}, 54.2%) and $BiVO_4$ (at 1.13 V_{RHE}, 37.4%). This was consistent with the higher onset potential of the electrode, and indicated that the Cu_2O layer facilitated charge separation. However, the water oxidation capacities of these materials were inferior, and charge transfer at the electrode-electrolyte interface was limited. Loading of the FeOOH/NiOOH OEC layer greatly improved charge transport at the interface. As the potential was increased, the transmission efficiency levelled off and no longer increased significantly, proving that the water oxidation reaction was close to saturation. Therefore, these results verified that the use of Cu_2O as the hole extraction layer and the FeOOH/NiOOH OEC layer in the $BiVO_4/Cu_2O$/FeOOH/NiOOH system synergistically promoted charge separation and transport, thus improving the PEC performance.

Additionally, the Mott–Schottky diagram enabled determination of the type of semiconductor and verified the presence of an internal electric field. As shown in Fig. S7a, b, $BiVO_4$ had a positive slope, indicating that it is a typical n-type semiconductor, while Cu_2O had a negative slope, indicating that it is

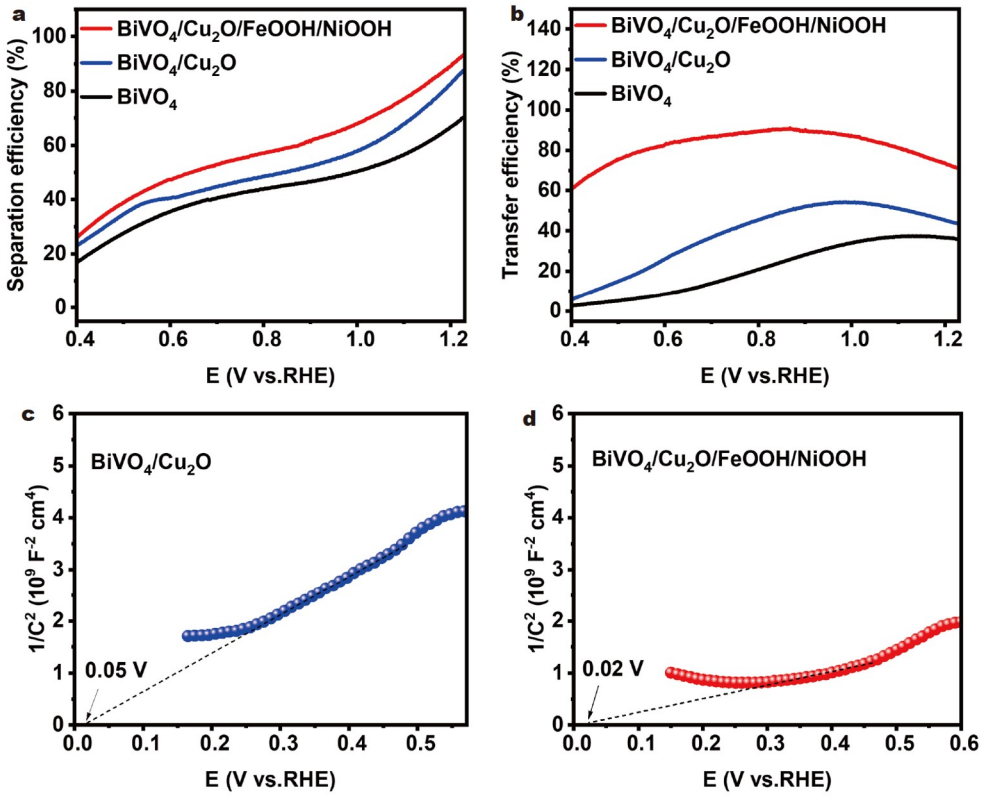

Figure 6 (a) η_{sep} and (b) η_{trans} of $BiVO_4$, $BiVO_4/Cu_2O$ and $BiVO_4/Cu_2O$/FeOOH/NiOOH photoanodes. Mott-Schottky plots of (c) $BiVO_4/Cu_2O$ and (d) $BiVO_4/Cu_2O$/FeOOH/NiOOH photoanodes.

a typical p-type semiconductor. Similarly, the flat band potential (E_{FB}) and carrier density (N_D) were obtained from the Mott–Schottky equation:

$$1/C^2 = 2/(e\varepsilon\varepsilon_0 N_D) \times (E - E_{FB} - KT/e), \quad (6)$$

where C is the space charge region capacitance (F cm^{-2}), ε is the relative dielectric constant (for $BiVO_4$ is 68), ε_0 is the absolute dielectric constant (8.85×10^{-12} F m^{-1}), K is the Boltzmann constant (1.38×10^{-23} F m^{-1}), and T is the absolute temperature (K) [43].

Notably, compared with those of the pure $BiVO_4$ photoanode (Fig. S7b), the flat band potentials of $BiVO_4/Cu_2O$ (Fig. 6c) and $BiVO_4/Cu_2O$/FeOOH/NiOOH (Fig. 6d) were significantly shifted in the negative direction, implying that photoexcited electron–hole recombination was suppressed. The calculated carrier densities of the $BiVO_4$, $BiVO_4/Cu_2O$ and $BiVO_4/Cu_2O$/FeOOH/NiOOH photoanodes were 1.1×10^{22}, 2.0×10^{22} and 4.5×10^{22} cm^{-3}, respectively. These results showed that the Cu_2O layer separated the photogenerated electrons and holes and prolonged the carrier lifetime. In addition, the holes on the electrode/electrolyte surface were transferred and consumed in time after addition of the cocatalyst FeOOH/NiOOH, which suppressed recombination of the electron–hole pairs [60].

The mechanism proposed for charge transfer on the $BiVO_4/Cu_2O$/FeOOH/NiOOH photoanode is show in Fig. 7. From the UV-vis absorption spectra of $BiVO_4$ and Cu_2O (Fig. S8a, b), the bandgaps of $BiVO_4$ and Cu_2O were estimated to be 2.56 and 2.00 eV, respectively (insets in Fig. S8c, d). The positions of the VB of $BiVO_4$ and Cu_2O were calculated with the following equations:

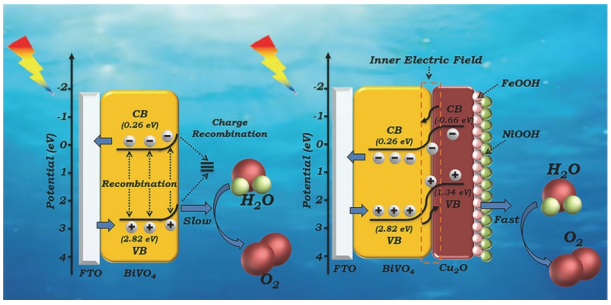

Figure 7 Mechanism of charge transfer on the $BiVO_4/Cu_2O$/FeOOH/NiOOH photoanode.

$$E_{VB} = X - E_e + 0.5E_g, \quad (7)$$

$$E_{CB} = E_{VB} - E_g, \quad (8)$$

where E_e is the energy of free electrons on the hydrogen scale (~4.5 eV), E_g is the bandgap and X is the absolute electronegativity of the semiconductor. The X values for Cu_2O and $BiVO_4$ are ~4.840 and 6.035 eV [61], respectively. The E_g values for Cu_2O and $BiVO_4$ are ~2.00 and 2.56 eV, respectively.

The calculated VB and CB energies for n-type $BiVO_4$ were 2.82 and 0.26 eV, respectively, while the calculated VB and CB energies for p-type Cu_2O were 1.34 and −0.66 eV, respectively. Under illumination, $BiVO_4$ absorbed photons to generate electrons and holes, but the photoinduced charge recombined rapidly. When the p-type Cu_2O coupled with n-type $BiVO_4$ formed an internal electric field, $BiVO_4$ was excited to produce hole and electron pairs, and the photogenerated electrons were

isolated by the Cu_2O layer; this led to rapid transfer of the extracted photogenerated holes to the FeOOH/NiOOH OEC layer, thus accelerating the rate of water oxidation. Therefore, in this device, Cu_2O served as a hole extraction layer that transferred holes from the $BiVO_4$ photoanode to the OEC layer.

CONCLUSIONS

In summary, we synthesized an efficient $BiVO_4$ photoanode by introducing a Cu_2O hole extraction layer. The influence of the Cu_2O layer thickness on the hole extraction was explored and optimized. The photocurrent densities of the $BiVO_4$/Cu_2O/FeOOH/NiOOH photoanodes (3.85 mA cm^{-2} at 1.23 V_{RHE}) were 2.77 times greater than that of pure $BiVO_4$ (1.39 mA cm^{-2}). At 1.23 V_{RHE} (420 nm), the IPCE reached 23.5%, which was 4.2 times greater than that of pure $BiVO_4$ (5.6%). The hole extraction capability of the Cu_2O layer and the strong synergistic interaction between Cu_2O and the FeOOH/NiOOH OEC layer were the main reasons for the excellent PEC performance. Our work reveals the potential of applying Cu_2O in the photoanodes for solar conversion devices with strongly coupled interfaces.

Received 27 November 2023; accepted 19 January 2024; published online 12 April 2024

1 Kim JH, Lee JS. Elaborately modified $BiVO_4$ photoanodes for solar water splitting. Adv Mater, 2019, 31: 1806938
2 Zhong W, Wu X, Liu Y, *et al.* Simultaneous realization of sulfur-rich surface and amorphous nanocluster of NiS_{1+x} cocatalyst for efficient photocatalytic H_2 evolution. Appl Catal B-Environ, 2021, 280: 119455
3 Fujishima A, Honda K. Electrochemical photolysis of water at a semiconductor electrode. Nature, 1972, 238: 37–38
4 Grätzel M. Photoelectrochemical cells. Nature, 2001, 414: 338–344
5 Higashi T, Nishiyama H, Nandal V, *et al.* Design of semitransparent tantalum nitride photoanode for efficient and durable solar water splitting. Energy Environ Sci, 2022, 15: 4761–4775
6 Ding C, Shi J, Wang Z, *et al.* Photoelectrocatalytic water splitting: Significance of cocatalysts, electrolyte, and interfaces. ACS Catal, 2016, 7: 675–688
7 Moniz SJA, Shevlin SA, Martin DJ, *et al.* Visible-light driven heterojunction photocatalysts for water splitting—A critical review. Energy Environ Sci, 2015, 8: 731–759
8 Ma Z, Song K, Wang L, *et al.* WO_3/$BiVO_4$ type-II heterojunction arrays decorated with oxygen-deficient ZnO passivation layer: A highly efficient and stable photoanode. ACS Appl Mater Interfaces, 2019, 11: 889–897
9 Cui C, Heggen M, Zabka WD, *et al.* Atomically dispersed hybrid nickel-iridium sites for photoelectrocatalysis. Nat Commun, 2017, 8: 1341
10 Zhou T, Li L, Li J, *et al.* Electrochemically reduced TiO_2 photoanode coupled with oxygen vacancy-rich carbon quantum dots for synergistically improving photoelectrochemical performance. Chem Eng J, 2021, 425: 131770
11 Xiao F, Zhou W, Sun B, *et al.* Engineering oxygen vacancy on rutile TiO_2 for efficient electron-hole separation and high solar-driven photocatalytic hydrogen evolution. Sci China Mater, 2018, 61: 822–830
12 He D, Song X, Ke Z, *et al.* Construct Fe^{2+} species and Au particles for significantly enhanced photoelectrochemical performance of α-Fe_2O_3 by ion implantation. Sci China Mater, 2017, 61: 878–886
13 Wang L, Nguyen NT, Huang X, *et al.* Hematite photoanodes: Synergetic enhancement of light harvesting and charge management by sandwiched with Fe_2TiO_5/Fe_2O_3/Pt structures. Adv Funct Mater, 2017, 27: 1703527
14 Shao C, Chen R, Zhao Y, *et al.* Reducing the surface defects of Ta_3N_5 photoanode towards enhanced photoelectrochemical water oxidation. J Mater Chem A, 2020, 8: 23274–23283
15 Fu J, Fan Z, Nakabayashi M, *et al.* Interface engineering of Ta_3N_5 thin film photoanode for highly efficient photoelectrochemical water splitting. Nat Commun, 2022, 13: 729
16 Lv Z, Meng L, Cao F, *et al.* Wrapping $BiVO_4$ with chlorophyll for greatly improved photoelectrochemical performance and stability. Sci China Mater, 2022, 65: 1512–1521
17 Zhang J, Wei X, Zhao J, *et al.* Electronegative Cl^- modified $BiVO_4$ photoanode synergized with nickel hydroxide cocatalyst for high-performance photoelectrochemical water splitting. Chem Eng J, 2023, 454: 140081
18 Wang L, Zhang J, Li Y, *et al.* Heterostructured $CoFe_{1.5}Cr_{0.5}S_3O$/COFs/$BiVO_4$ photoanode boosts charge extraction for efficient photoelectrochemical water splitting. Appl Catal B-Environ, 2023, 336: 122921
19 Liu B, Li J, Wu HL, *et al.* Improved photoelectrocatalytic performance for water oxidation by earth-abundant cobalt molecular porphyrin complex-integrated $BiVO_4$ photoanode. ACS Appl Mater Interfaces, 2016, 8: 18577–18583
20 Trześniewski BJ, Digdaya IA, Nagaki T, *et al.* Near-complete suppression of surface losses and total internal quantum efficiency in $BiVO_4$ photoanodes. Energy Environ Sci, 2017, 10: 1517–1529
21 Zhang B, Zhang H, Wang Z, *et al.* Doping strategy to promote the charge separation in $BiVO_4$ photoanodes. Appl Catal B-Environ, 2017, 211: 258–265
22 Wu H, Zhang L, Qu S, *et al.* Polaron-mediated transport in $BiVO_4$ photoanodes for solar water oxidation. ACS Energy Lett, 2023, 8: 2177–2184
23 Gao RT, Wang L. Stable cocatalyst-free $BiVO_4$ photoanodes with passivated surface states for photocorrosion inhibition. Angew Chem Int Ed, 2020, 59: 23094–23099
24 Huang ZF, Pan L, Zou JJ, *et al.* Nanostructured bismuth vanadate-based materials for solar-energy-driven water oxidation: A review on recent progress. Nanoscale, 2014, 6: 14044–14063
25 Cao H, Wang T, Li J, *et al.* A molecular cobaloxime cocatalyst and ultrathin FeOOH nanolayers co-modified $BiVO_4$ photoanode for efficient photoelectrochemical water oxidation. J Energy Chem, 2022, 69: 497–505
26 Liang Y, Tsubota T, Mooij LPA, *et al.* Highly improved quantum efficiencies for thin film $BiVO_4$ photoanodes. J Phys Chem C, 2011, 115: 17594–17598
27 Wang L, Zhu J, Liu X. Oxygen-vacancy-dominated cocatalyst/hematite interface for boosting solar water splitting. ACS Appl Mater Interfaces, 2019, 11: 22272–22277
28 Liu Q, Chen C, Wei Y, *et al.* Photoelectrochemical water oxidation and methylene blue degradation enhanced by Nb doping and CoPi modification for hematite photoanodes. J Alloys Compd, 2023, 947: 169673
29 Gao RT, He D, Wu L, *et al.* Towards long-term photostability of nickel hydroxide/$BiVO_4$ photoanodes for oxygen evolution catalysts *via in situ* catalyst tuning. Angew Chem Int Ed, 2020, 59: 6213–6218
30 Lu X, Ye K, Zhang S, *et al.* Amorphous type FeOOH modified defective $BiVO_4$ photoanodes for photoelectrochemical water oxidation. Chem Eng J, 2022, 428: 131027
31 Tang F, Cheng W, Su H, *et al.* Smoothing surface trapping states in 3D coral-like CoOOH-wrapped-$BiVO_4$ for efficient photoelectrochemical water oxidation. ACS Appl Mater Interfaces, 2018, 10: 6228–6234
32 Zhang J, Huang Y, Lu X, *et al.* Enhanced $BiVO_4$ photoanode photoelectrochemical performance *via* borate treatment and a $NiFeO_x$ cocatalyst. ACS Sustain Chem Eng, 2021, 9: 8306–8314
33 Yu F, Li F, Yao T, *et al.* Fabrication and kinetic study of a ferrihydrite-modified $BiVO_4$ photoanode. ACS Catal, 2017, 7: 1868–1874
34 Ning X, Lu B, Zhang Z, *et al.* An efficient strategy for boosting photogenerated charge separation by using porphyrins as interfacial charge mediators. Angew Chem Int Ed, 2019, 58: 16800–16805
35 Zhong M, Hisatomi T, Kuang Y, *et al.* Surface modification of CoO_x loaded $BiVO_4$ photoanodes with ultrathin p-type NiO layers for improved solar water oxidation. J Am Chem Soc, 2015, 137: 5053–5060
36 Chang X, Wang T, Zhang P, *et al.* Enhanced surface reaction kinetics and charge separation of p–n heterojunction Co_3O_4/$BiVO_4$ photoanodes. J Am Chem Soc, 2015, 137: 8356–8359

37 Pan Q, Zhang C, Xiong Y, *et al.* Boosting charge separation and transfer by Plasmon-enhanced $MoS_2/BiVO_4$ p–n heterojunction composite for efficient photoelectrochemical water splitting. ACS Sustain Chem Eng, 2018, 6: 6378–6387
38 Soltani T, Tayyebi A, Lee BK. $BiFeO_3/BiVO_4$ p-n heterojunction for efficient and stable photocatalytic and photoelectrochemical water splitting under visible-light irradiation. Catal Today, 2020, 340: 188–196
39 He P, Shen X, Gao H. Size-controlled preparation of Cu_2O octahedron nanocrystals and studies on their optical absorption. J Colloid Interface Sci, 2005, 284: 510–515
40 McDonald KJ, Choi KS. A new electrochemical synthesis route for a BiOI electrode and its conversion to a highly efficient porous $BiVO_4$ photoanode for solar water oxidation. Energy Environ Sci, 2012, 5: 8553–8557
41 Cembrero-Coca P, Cembrero J, Busquets-Mataix D, *et al.* Factorial electrochemical design for tailoring of morphological and optical properties of Cu_2O. Mater Sci Tech, 2017, 33: 2102–2109
42 Kim TW, Choi KS. Nanoporous $BiVO_4$ photoanodes with dual-layer oxygen evolution catalysts for solar water splitting. Science, 2014, 343: 990–994
43 Kim JH, Jo YH, Kim JH, *et al.* Ultrafast fabrication of highly active $BiVO_4$ photoanodes by hybrid microwave annealing for unbiased solar water splitting. Nanoscale, 2016, 8: 17623–17631
44 Li X, Wan J, Ma Y, *et al.* Study on cobalt-phosphate (Co-Pi) modified $BiVO_4/Cu_2O$ photoanode to significantly inhibit photochemical corrosion and improve the photoelectrochemical performance. Chem Eng J, 2020, 404: 127054
45 Zhang Y, Xu L, Liu B, *et al.* Engineering $BiVO_4$ and oxygen evolution cocatalyst interfaces with rapid hole extraction for photoelectrochemical water splitting. ACS Catal, 2023, 13: 5938–5948
46 Yang L, Wang R, Chu D, *et al.* $BiVO_4$ photoelectrodes for unbiased solar water splitting devices enabled by electrodepositing of Cu_2O simultaneously as photoanode and photocathode. J Alloys Compd, 2023, 945: 169336
47 Chen M, Chang X, Li C, *et al.* Ni-doped $BiVO_4$ photoanode for efficient photoelectrochemical water splitting. J Colloid Interface Sci, 2023, 640: 162–169
48 Zhang Z, Huang X, Zhang B, *et al.* High-performance and stable $BiVO_4$ photoanodes for solar water splitting *via* phosphorus–oxygen bonded FeNi catalysts. Energy Environ Sci, 2022, 15: 2867–2873
49 Zheng JH, Jiang Q, Lian JS. Synthesis and optical properties of flower-like ZnO nanorods by thermal evaporation method. Appl Surf Sci, 2011, 257: 5083–5087
50 Wang Q, Wu X, Zhang L. Designed of bifunctional Z-scheme $CuSnO_3@Cu_2O$ heterojunctions film for photoelectrochemical catalytic reduction and ultrasensitive sensing nitrobenzene. Chem Eng J, 2019, 361: 398–407
51 Zhang B, Wang L, Zhang Y, *et al.* Ultrathin FeOOH nanolayers with abundant oxygen vacancies on $BiVO_4$ photoanodes for efficient water oxidation. Angew Chem Int Ed, 2018, 57: 2248–2252
52 Liang H, Lin J, Jia H, *et al.* Hierarchical NiCo-LDH@NiOOH core-shell heterostructure on carbon fiber cloth as battery-like electrode for supercapacitor. J Power Sources, 2018, 378: 248–254
53 Ye S, Ding C, Chen R, *et al.* Mimicking the key functions of photosystem II in artificial photosynthesis for photoelectrocatalytic water splitting. J Am Chem Soc, 2018, 140: 3250–3256
54 Kudo A, Omori K, Kato H. A novel aqueous process for preparation of crystal form-controlled and highly crystalline $BiVO_4$ powder from layered vanadates at room temperature and its photocatalytic and photophysical properties. J Am Chem Soc, 1999, 121: 11459–11467
55 Bai S, Liu J, Cui M, *et al.* Two-step electrodeposition to fabricate the p–n heterojunction of a $Cu_2O/BiVO_4$ photoanode for the enhancement of photoelectrochemical water splitting. Dalton Trans, 2018, 47: 6763–6771
56 Zhang Y, Yi Z, Wu G, *et al.* Novel Y doped $BiVO_4$ thin film electrodes for enhanced photoelectric and photocatalytic performance. J Photochem PhotoBiol A-Chem, 2016, 327: 25–32
57 Wang F, Septina W, Chemseddine A, *et al.* Gradient self-doped $CuBi_2O_4$ with highly improved charge separation efficiency. J Am Chem Soc, 2017, 139: 15094–15103
58 Cui J, Daboczi M, Regue M, *et al.* 2D bismuthene as a functional interlayer between $BiVO_4$ and NiFeOOH for enhanced oxygen-evolution photoanodes. Adv Funct Mater, 2022, 32: 2207136
59 Zhang K, Jin B, Park C, *et al.* Black phosphorene as a hole extraction layer boosting solar water splitting of oxygen evolution catalysts. Nat Commun, 2019, 10: 2001
60 Bai S, Jia S, Zhao Y, *et al.* NiFePB-modified $ZnO/BiVO_4$ photoanode for PEC water oxidation. Dalton Trans, 2023, 52: 5760–5770
61 Wang W, Zhang W, Meng S, *et al.* Enhanced photoelectrochemical water splitting and photocatalytic water oxidation of Cu_2O nanocube-loaded $BiVO_4$ nanocrystal heterostructures. Electron Mater Lett, 2016, 12: 753–760

Acknowledgements This work was supported by the National Natural Science Foundation of China (22008165 and 21878201), the Natural Science Foundation of Shanxi Province (202303021211035), the 7th Youth Talent Support Program of Shanxi Province, and the Opening Project of Sichuan University of Science and Engineering, Material Corrosion and Protection Key Laboratory of Sichuan Province (2021CL22).

Author contributions Wang X and Ma Z conceived the project. Tian Z performed the experiments and wrote the draft with help from Wang Z and Li J. All authors contributed to the general discussion.

Conflict of interest The authors declare that they have no conflict of interest.

Supplementary information Supporting data are available in the online version of the paper.

Ze Tian is currently a master candidate at the College of Material Science and Engineering, Taiyuan University of Technology. His research focuses on the preparation and photoelectrochemical performance of $BiVO_4$-based photoanodes.

Zizai Ma is now working at the College of Chemistry, Taiyuan University of Technology. She received her PhD degree from Taiyuan University of Technology in 2019. From 2020 to 2021, she worked as a postdoc researcher at Taiyuan University of Technology. Her research interests focus on novel energy materials for electrocatalysis and photoelectrocatalysis.

Xiaoguang Wang is a professor at the College of Material Science and Engineering, Taiyuan University of Technology. He obtained his PhD degree from Shandong University in 2011. From 2014 to 2015, he worked as a Marie Curie Cofund Research Fellow postdoc at the International Iberian Nanotechnology Laboratory. His current research interests focus on the synthesis and regulation of novel nanostructured materials for energy storage and conversion.

Cu_2O作为空穴提取层修饰$BiVO_4$光阳极以增强电荷分离和转移

田泽[1], 王振霞[1], 马自在[2,3*], 李晋平[3], 王孝广[1,3*]

摘要 光生电荷的分离和转移被认为是影响$BiVO_4$基光阳极光电性能的核心因素之一. 本文设计了在$BiVO_4$光阳极与析氧助催化剂之间插入空穴提取层的方法. Cu_2O作为空穴提取层引入到助催化剂层(FeOOH/NiOOH)和$BiVO_4$之间, 可以有效优化空穴的迁移路径, 延长光生空穴的寿命, 从而提高电极的光电化学性能. 与$BiVO_4$相比, 调整后的$BiVO_4$/Cu_2O/FeOOH/NiOOH光阳极的电荷分离效率从70.6%提高到了92.0%. 此外, 该光阳极在1.23 V_{RHE} (AM 1.5G 照明下)下, 还显示出了3.85 mA cm^{-2}的高光电流密度, 是$BiVO_4$的2.77倍. 我们的研究结果表明, 电沉积Cu_2O空穴提取层是一种简单且可扩展的方法, 能够有效提高$BiVO_4$的光电活性, 可用于太阳能驱动水分解领域.